

# Elastic anomalies associated with domain switching in BaTiO<sub>3</sub> single crystals under *in situ* electrical cycling

Cite as: APL Mater. 7, 051109 (2019); <https://doi.org/10.1063/1.5088749>

Submitted: 14 January 2019 . Accepted: 15 April 2019 . Published Online: 21 May 2019

D. Pesquera , B. Casals , J. E. Thompson, G. F. Nataf , X. Moya , and M. A. Carpenter



View Online



Export Citation



CrossMark

## ARTICLES YOU MAY BE INTERESTED IN

Atomically interface engineered micrometer-thick SrMoO<sub>3</sub> oxide electrodes for thin-film Ba<sub>x</sub>Sr<sub>1-x</sub>TiO<sub>3</sub> ferroelectric varactors tunable at low voltages

APL Materials 7, 051107 (2019); <https://doi.org/10.1063/1.5094855>


Large tetragonality and room temperature ferroelectricity in compressively strained CaTiO<sub>3</sub> thin films

APL Materials 7, 051104 (2019); <https://doi.org/10.1063/1.5090798>

Barrier materials for flexible bioelectronic implants with chronic stability—Current approaches and future directions

APL Materials 7, 050902 (2019); <https://doi.org/10.1063/1.5094415>

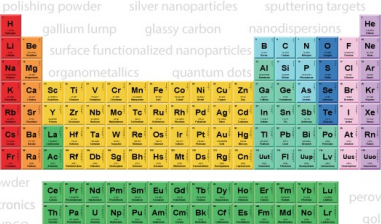
additive manufacturing epitaxial crystal growth cerium oxide polishing powder silver nanoparticles sputtering targets



THE ADVANCED MATERIALS MANUFACTURER®

deposition slugs OLED Lighting spintronics solar energy osmium nanoribbons thin films chalcogenides AuNPs GDC li-ion battery electrolytes 99.999% ruthenium spheres

endoheedral fullerenes copper nanoparticles diamond micropowder CIGS MBE grade materials palladium catalysts flexible electronics beta-barium borate borosilicate glass dysprosium pellets YBCO pyrolytic graphite 3d graphene foam indium tin oxide mesoporous silica raman substrates sapphire windows tungsten carbide InGaAs barium fluoride carbon nanotubes lithium niobate scandium powder



gallium lump glassy carbon nanodispersions III-IV semiconductors CVD precursors europium phosphors InAs wafers laser crystals ultra high purity materials MOFs rare earth metals photovoltaics refractory metals MOCVD superconductors transparent ceramics ultra high purity silicon

organometallics quantum dot

American Elements opens up a world of possibilities so you can **Now Invent!**

Over 15,000 certified high purity laboratory chemicals, metals, & advanced materials and a state-of-the-art Research Center. Printable GHS-compliant Safety Data Sheets. Thousands of new products. And much more. All on a secure multi-language "Mobile Responsive" platform.

perovskite crystals yttrium iron garnet alternative energy h-BN gold nanocubes graphene oxide macromolecules photonics rhodium sponge fiber optics beamsplitters infrared dyes zeolites fused quartz metallocenes platinum ink buckyballs Ti-6Al-4V

**Now Invent.™**  
The Next Generation of Material Science Catalogs

[www.americanelements.com](http://www.americanelements.com)

# Elastic anomalies associated with domain switching in BaTiO<sub>3</sub> single crystals under *in situ* electrical cycling

Cite as: APL Mater. 7, 051109 (2019); doi: 10.1063/1.5088749

Submitted: 14 January 2019 • Accepted: 15 April 2019 •

Published Online: 21 May 2019



View Online



Export Citation



CrossMark

D. Pesquera,<sup>1,a)</sup> B. Casals,<sup>1</sup> J. E. Thompson,<sup>2</sup> G. F. Nataf,<sup>2</sup> X. Moya,<sup>2</sup> and M. A. Carpenter<sup>1</sup>

## AFFILIATIONS

<sup>1</sup>Department of Earth Sciences, University of Cambridge, Downing Street, Cambridge CB2 3EQ, United Kingdom

<sup>2</sup>Department of Materials Science, University of Cambridge, 27 Charles Babbage Road, Cambridge CB3 0FS, United Kingdom

<sup>a)</sup>dpesquera@cantab.net

## ABSTRACT

The elastic response of BaTiO<sub>3</sub> single crystals during electric field cycling at room temperature has been studied using *in situ* Resonant Ultrasound Spectroscopy (RUS), which allows monitoring of both the elastic and anelastic changes caused by ferroelectric polarization switching. We find that the first ferroelectric switching of a virgin single crystal is dominated by ferroelastic 90° switching. In subsequent ferroelectric switching, ferroelastic switching is reduced by domain pinning and by the predominance of 180° ferroelectric domains, as confirmed by polarized light microscopy. RUS under *in situ* electric field therefore demonstrates to be an effective technique for the investigation of electromechanical coupling in ferroelectrics.

© 2019 Author(s). All article content, except where otherwise noted, is licensed under a Creative Commons Attribution (CC BY) license (<http://creativecommons.org/licenses/by/4.0/>). <https://doi.org/10.1063/1.5088749>

The process of polarization switching in ferroelectrics is generally not homogeneous and involves nucleation and growth of domains.<sup>1,2</sup> In prototypical tetragonal ferroelectrics, such as BaTiO<sub>3</sub> at room temperature, two kinds of ferroelectric domains can nucleate:<sup>3</sup> 180° domains with polarizations antiparallel to each other, which minimize depolarization fields, and 90° domains with polarizations orthogonal to each other, which minimize strain via the formation of twins. During electrical poling, local strains are generated when 90° domains switch but not when 180° domains switch. Limiting the mobility of domain walls by introducing specific point defects and domain engineering has proven an effective strategy to enhance piezoelectricity in BaTiO<sub>3</sub>.<sup>4,5</sup> Large strains are desirable, e.g., to achieve giant magnetoelectric effects in multiferroic composites,<sup>6–10</sup> and polarization switching without domain propagation is preferred for ferroelectric memory devices.<sup>11,12</sup> Separately, domain wall pinning and domain jamming may cause fatigue effects in ferroelectrics, hampering polarization switching upon repeated voltage cycling, ultimately limiting the performance of devices.<sup>13,14</sup> Understanding the role of the domain structure on ferroelectric switching is thus of high technological relevance for the optimization of devices based on ferroelectric crystals. BaTiO<sub>3</sub> has been the

subject of many such studies for more than 50 years:<sup>15–23</sup> some focused on the strain coupling with polarization switching<sup>20,22,23</sup> and some on the microstructure evolution with electric field.<sup>15–19,21</sup> However, combined experiments showing the link between both aspects are lacking.

Resonant Ultrasound Spectroscopy (RUS) is a convenient technique for determining the elastic constants of solids. Since the elastic constants are second derivatives of the free energy, their evolution as a function of external stimuli provides a highly sensitive indicator of strain coupling with the driving order parameter of a phase transition.<sup>24</sup> Moreover, the small dynamic stress that is applied to the sample during RUS is well suited for exploring relaxation mechanisms in the elastic regime and for studying dissipation processes due to microstructural dynamics as associated with e.g., twin-wall motion.<sup>25,26</sup> RUS has also proved to be an effective tool for identifying thermally driven energy dissipation associated with the existence of polar nanoregions in BaTiO<sub>3</sub><sup>27</sup> and relaxors,<sup>28,29</sup> but the elastic and anelastic responses under *in situ* electrical cycling remain unexplored.

Here, we report, for the first time, RUS measurements under *in situ* electric field in the prototypical ferroelectric BaTiO<sub>3</sub>. We show

that this technique allows for the identification of strain and energy dissipation caused by ferroelectric switching processes. We find that both strain and dissipation are large upon the first electrical poling, but gradually disappear after a few electrical switches, suggesting a reduced contribution of ferroelastic switching and a freezing of domain dynamics, under sustained operation. Complementary *in situ* studies of domain distribution using polarized light microscopy reveal the evolution from initially predominant  $90^\circ$  switching via twin walls motion, to localized  $180^\circ$  switching, limited by domain pinning around defects and locally strained regions. These observations are in agreement with the results obtained from RUS, thus demonstrating the potential of RUS to explore ferroelectric switching mechanisms.

The RUS data and optical images reported here were taken on two different pieces (labeled samples A and B) of an optically transparent electrically virgin  $\text{BaTiO}_3$  single crystal (MaTeCK), which was cut using a fine annular diamond saw. Each piece had approximate dimensions of  $3 \text{ mm} \times 3 \text{ mm} \times 0.5 \text{ mm}$ , with edges parallel to  $\langle 100 \rangle$  crystallographic axes. Initial optical examination using a Zeiss Axioplan 1 optical microscope in transmission mode under crossed polarizers, and a digital camera, revealed that both samples presented a similar configuration of micron-size domains with boundaries parallel to  $[100]$ , evidencing a mixed microstructure consisting of  $a$  domains (with polarization vectors along  $[100]$  or  $[010]$ ) and  $c$  domains (with polarization vectors along  $[001]$ ).

For RUS measurements under electric field, sample A was held by two opposite corners between two piezoelectric transducers.  $20 \mu\text{m}$ -thick copper wires were attached to the two large surfaces parallel to  $(001)$  using RS-PRO silver conducting paint as electrodes. DC voltage was applied to the sample via the core and the shield of a coaxial cable connected to a Keithley 2260B power supply. At each value of applied voltage, mechanical resonances of the crystal in the frequency range  $400\text{--}1300 \text{ kHz}$  were measured using a lock-in amplifier (Stanford, model SR830).<sup>30</sup>

For optical microscopy under electric field,  $\sim 200 \text{ nm}$  thick transparent  $\text{InTiO}_3$  electrodes were deposited at a base pressure  $< 10^{-8} \text{ mbar}$  using magnetron sputtering ( $20 \text{ W}$ ,  $2.5 \text{ Pa Ar}$ ) on both  $(001)$  surfaces of sample B. During the imaging, an increasing voltage was applied across the sample at a rate of  $0.3 \text{ V/s}$  using a Keithley 6487 picoammeter, which also allowed the displacement current in the sample to be recorded.

In RUS experiments on single crystals, the frequencies of individual mechanical resonances are determined by combinations of elastic constants, with a predominant contribution from shear modes. For the first two electrical cycles, Figs. 1(a) and 1(b) shows the evolution of a resonance peak in sample A that does not interfere with adjacent peaks. Other peaks were found to display the same qualitative evolution with applied voltage. The results of fitting this peak with an asymmetric Lorentzian function are given in Figs. 1(c) and 1(d), as (i) values of the squared resonance frequency,  $f^2$ , which scale with the elastic constants and (ii) the inverse mechanical quality factor  $Q^{-1} = \Delta f/f$ , which is a measure of acoustic attenuation ( $\Delta f$  is the peak full width at half maximum). A pronounced softening of the elastic constants with increasing electric fields is evident upon the first poling of the crystal. The onset of this softening occurs simultaneously with a sharp peak in the acoustic dissipation at the coercive field  $E_c \approx 0.4 \text{ kV/cm}$ . On further increasing field, the crystal stiffens (increase in  $f^2$ ) and a wider peak in the dissipation is

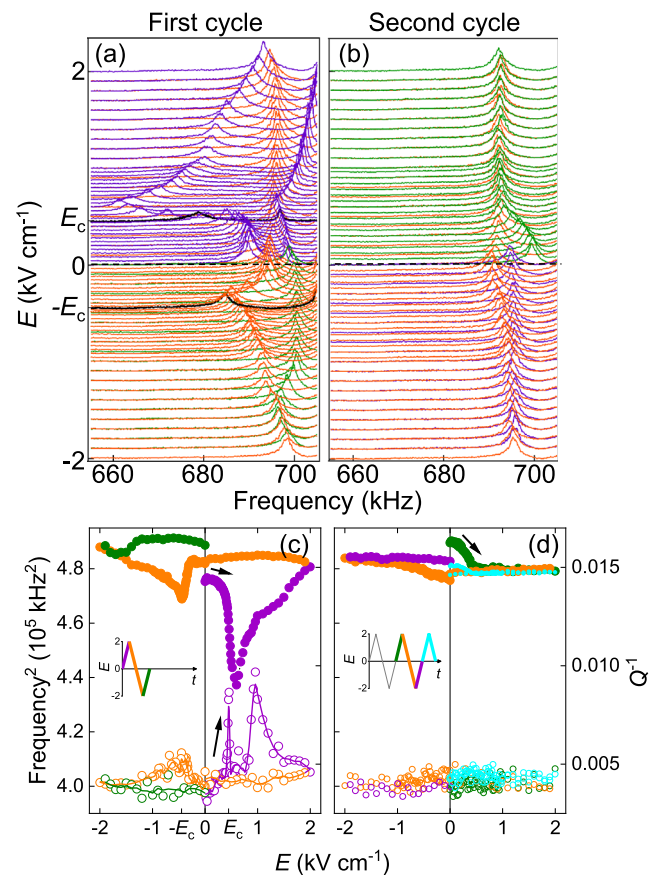


**FIG. 1.** Detail of the electric-field evolution of RUS spectra during (a) first and (b) second electrical cycles in an initially electrically virgin  $\text{BaTiO}_3$  crystal (sample A). Each spectrum has been offset up the y-axis in proportion to the voltage applied to the sample during the acquisition of the spectrum. Spectra colors indicate the field ramp step as shown in (c) and (d); black spectra in (a) correspond to spectra taken at  $\pm E_c$  on increasing field. Dependence with applied field of  $f^2$  (left axis, closed circles) and  $Q^{-1}$  (right axis, open circles) from fits to the resonance peaks in (a,b) are shown in (c) and (d). Insets show the applied field sequence.

observed around  $2E_c$ . When approaching the highest applied field ( $2 \text{ kV/cm}$ ), the initial resonance frequency and attenuation values are recovered, and these values are preserved after removing the voltage. When reversing the electric field, a smaller elastic softening and a smaller increase in the acoustic loss are evidenced, as revealed by a minimum in  $f^2$  and a maximum in  $Q^{-1}$  around  $-E_c$ , respectively.

The butterfly-shaped curve observed in the initial cycle is modified in the second electrical cycle [Fig. 1(d)], where a softening at  $+E_c$  is only partially compensated when applying a negative field. In this second cycle, acoustic losses remained constant and below 0.5%. Further cycling the electric field yielded smaller changes in the elastic constants [cyan points in Fig. 1(d)] and negligible variations in the attenuation.

While the DC applied voltage can move both  $90^\circ$  and  $180^\circ$  twin walls because both are ferroelectric, the small dynamic stress

applied during RUS measurements only swings  $90^\circ$  walls as they are ferroelastic ( $180^\circ$  walls are unaffected as the shear strain is identical in the neighboring domains). Therefore, RUS only probes the elastic and anelastic changes associated with  $90^\circ$  twin walls. In this light, we can interpret the results presented above as an evolution of the twin wall population from an initial state dominated by  $90^\circ$  walls (which can be either  $a$ - $a$  or  $a$ - $c$ ) to a final state with predominantly  $180^\circ$  walls ( $c$ - $c$ ). The initial poling causes the motion of  $90^\circ$  twin walls, hence inducing an elastic softening. The two peaks observed in the acoustic loss indicate the occurrence of two domain switching processes taking place during the first cycling. When the twin walls reach new equilibrium positions, or  $a$  domains transform into  $c$  domains, the dissipation is reduced and the crystal stiffens. In the process of polarization reversal, a single broad softening and loss peak indicate ferroelastic switching around  $-E_c$ . However, on successive cycling, RUS spectra evidence frozen dynamics and minor changes in the elastic constants, pointing to increased domain pinning and/or predominant nonferroelastic  $180^\circ$  switching. We note that wall mobility is only recovered after annealing the crystal above  $T_c$ , as shown in the [supplementary material](#).

In order to understand the microscopic mechanism behind the observed evolution of the elastic constants and acoustic dissipation, we imaged sample B through the surfaces parallel to (001), while sweeping the applied voltage [Fig. 2(a) and videos in the [supplementary material](#)] and simultaneously measuring the displacement current [Figs. 2(b) and 2(c)].  $90^\circ$  domains in the virgin crystal were clearly visible due to the birefringence contrast between them: dark regions showing no birefringence contrast correspond to  $c$  domains, while bright regions correspond to  $a$  domains. The crossed polarizers were adjusted at  $45^\circ$  from the main crystallographic axes to maximize the contrast. In the initial state (step 1), all domain walls were aligned with the [100] axis. Regions with large  $a$  domains and  $c$  domains can be seen at the bottom of the image, while a pattern of fine  $a$ - $c$  domains is seen at the top. Such domain width variations across the crystal were also observed in sample A and may be evidence of an inhomogeneous distribution of defects.<sup>31</sup>

When an electric field was applied during initial poling, the large  $a$  domain was swept away (step 2) and merged completely with the bottom  $c$  domain at a field  $E_c \approx 0.4$  kV/cm. Further increasing the voltage above  $2E_c$  caused a widening of the top  $a$ - $c$  domains and jerky movements of birefringent regions away from

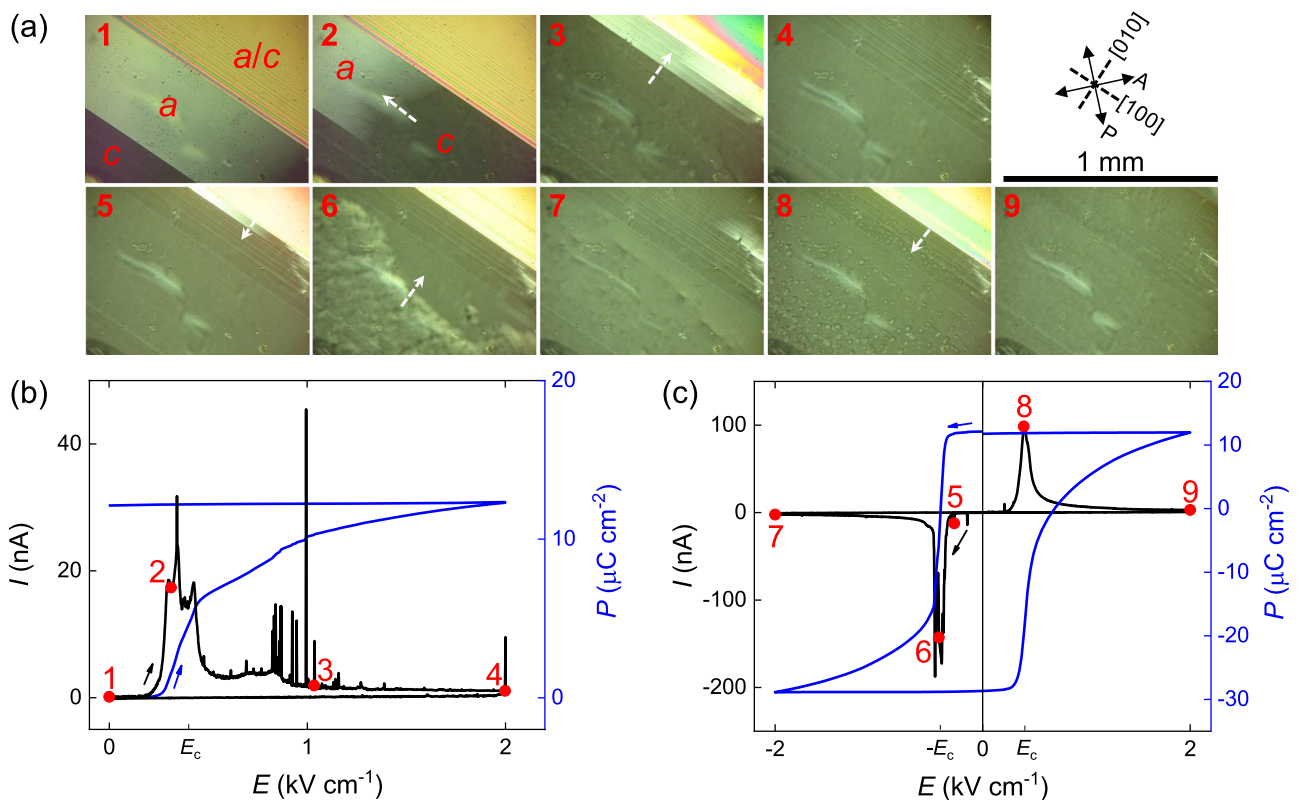


**FIG. 2.** (a) Snapshots of a region of sample B during electrical cycling, taken at steps indicated in (b) and (c), using light transmitted along the [001] direction of the crystal and crossed polarizers, both at  $45^\circ$  from the main in-plane (100) axes (see sketch at top right corner). The voltage was applied along [001] through transparent  $\text{InTiO}_3$  electrodes deposited on opposite sides of the crystal. Labels in panels 1 and 2 indicate the orientations of  $\text{BaTiO}_3$  domains, with  $a$  domains having polarization along [010], and  $c$  domains having polarization along [001]. White dashed arrows indicate the observed domain-wall propagation during electrical cycling (see the videos in the [supplementary material](#) for the complete evolution of the domain structure under field). (b) Electric-field ( $E$ ) dependence of displacement current  $I$  (black, left axis), and corresponding polarization  $P$  (blue, right axis) during the initial poling. (c)  $I(E)$  (left axis) and  $P(E)$  (right axis) for a complete electrical cycle after the first poling.



the  $c$  macrodomain (step 3, [supplementary material](#), Video 1). More subtly, a number of bubblelike domains nucleated in the  $c$  macrodomain, suggesting some minority  $180^\circ$  switching<sup>32</sup> that became more evident in the following electrical cycles. At the highest field, no color contrast was observed, as expected for a single  $c$  domain state, although weak contrast from the  $a$ - $c$  pattern could still be observed at the top of the image (panel 4). This may correspond to pinned domains, likely localized at the surface of the crystal.<sup>33</sup>

The displacement current measurements [Fig. 2(b)] confirm that initial poling of the sample is dominated by two polarization switching events, as revealed by a large current peak at  $E_c$ , followed by a number of smaller current jerks around  $2E_c$ . Both processes can be correlated with the ferroelastic switching events observed in the optical images, corresponding to displacement of domain walls due to the  $90^\circ$  switching from a multidomain  $a$ - $c$  structure to a nominally single  $c$  domain (see the [supplementary material](#), Video 1 for the complete poling process).

The process of polarization reversal is illustrated in steps 5–7 of Fig. 2(a) (shown fully in the [supplementary material](#), Video 2). An increase in the birefringence, with simultaneous multiple peaks in the switching current [Fig. 2(c)], indicates nucleation of  $a$ - $c$  domains in their previous locations. This is followed by the propagation of a corrugated structure toward the  $a$ - $c$  pattern (step 6), occurring at  $-E_c$  and producing a large peak in the current. This kind of structure is typically observed in the switching of antiparallel domains<sup>34,35</sup> and here provides evidence of the nucleation and propagation of  $180^\circ$  domain walls. During propagation, the front is slowed down by defects that act as pinning centers. At higher fields, the contrast becomes uniform, except for the remaining lines that arise from the  $a$ - $c$  surface pattern, and increased texturing in the whole area (step 7). On reversing the voltage, the nucleation of  $a$ - $c$  domains follows mostly the previous behavior although the  $180^\circ$  switching in the  $c$  macro-domain occurs via nucleation of bubblelike domains with no propagation (see the [supplementary material](#), Video 3), favorably at the location of the defects that acted as nucleation centers (step 8). The alignment of these domains parallel to pre-existing domain walls suggests a nucleation mechanism via skyrmion domain ejection, as proposed by Dawber *et al.*<sup>36</sup> Nucleation occurs at the same time as the large increase in the displacement current [Fig. 2(c)]. Traces of these bubble domains could still be seen at the highest applied field (step 9), which may indicate the presence of localized regions of remanent strain.

To summarize the above observations, while in the first poling, most switching events occur via motion of  $90^\circ$  domain walls, evidencing their lower energy with respect to  $180^\circ$  walls,<sup>37</sup> in the electrical cycle that follows the first poling,  $180^\circ$  domain switching becomes the predominant source for polarization reversal although a significant contribution from ferroelastic switching is still noticeable in some regions of the sample. These results are consistent with previous observations in which  $180^\circ$  domain nucleation in poled crystals was found to be easier than  $90^\circ$  domain nucleation, due to strain constraints,<sup>34</sup> and with the observed reduction of acoustic emission signals in BaTiO<sub>3</sub> crystals after the first electrical cycle,<sup>23</sup> suggesting that  $90^\circ$  domain walls are more prone to pinning. The total polarization that switches reversibly in the electrical cycling shown in the first cycle is  $20.6 \mu\text{C}/\text{cm}^2$  [Figs. 1(b) and 1(c)].

On subsequent cycling, however, the switched polarization gradually drops, as evidenced by the decreasing amplitude of the

displacement current peak observed in the  $I$ - $V$  curves [Fig. 3(a)]. In the second and third cycle, the switched polarization is reduced by 44% and 76%, respectively [inset in Fig. 3(a)]. A significantly reduced domain motion was also identified in the optical images (see the [supplementary material](#), Video 4). When increasing the maximum electric field to 8 kV/cm, small current peaks still occur at  $\pm E_c$ , but much larger and broader peaks are observed around  $\pm 4$  kV/cm [Fig. 3(b)]. A large increase in the leakage current is also observed—likely caused by sample damage at high voltages—which prevents a reliable estimation of the switched polarization. During this higher-field electrical cycling, no clear signature of domain switching is identified in the images (see the [supplementary material](#), Video 5), which show a uniform structure of islets with edges partially aligned to the main in-plane crystallographic axes, and some regions of stripes parallel to [100] showing weak birefringence [inset

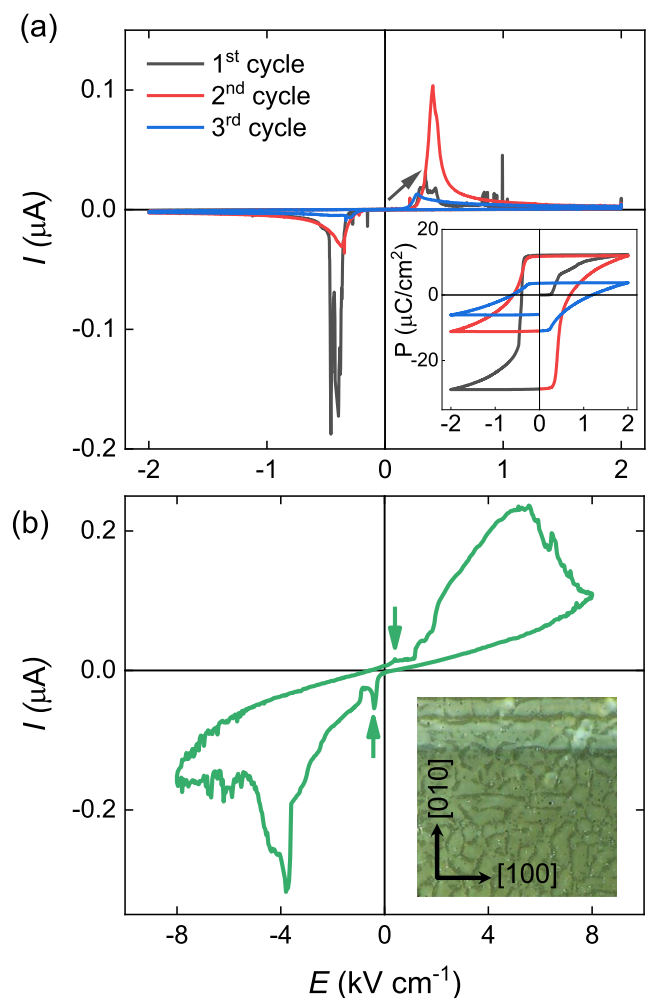


**FIG. 3.** (a) Displacement current during electrical cycling of sample B with a maximum electric field of 2 kV/cm. Inset: Polarization loops obtained from the integration of displacement current. (b) Displacement current vs electric field, when increasing the maximum field to 8 kV/cm; arrows indicate small current peaks observed at  $\pm E_c$ . The inset image shows a  $500 \times 500 \mu\text{m}$  region of the sample after repeated electrical cycling up to  $\pm 8$  kV/cm.

in Fig. 3(b)]. These observations suggest a structure dominated by pinned *c* domains, which switch uniformly at high fields (with no propagation) and some remaining areas of *a-c* domains, also pinned at the locations reached after the initial cycling of the crystal, which still switch at low field. Such observations point toward notable fatigue effects in our BaTiO<sub>3</sub> samples, likely induced by agglomeration of defects at domain walls during electrical cycling,<sup>38–40</sup> or electric field induced cracking,<sup>41</sup> which lead to domain wall pinning and increased coercive fields. We note that the fatigue effects that we observe in our samples may be dependent on measurement conditions (e.g., field frequency and amplitude) and sample dimensions (thicker crystals may be less affected by surface pinning and develop further ferroelastic switching<sup>23</sup>).

In summary, we have shown that RUS allows *in situ* monitoring of ferroelastic switching processes during electrical cycling of ferroelectric crystals. Large changes in elastic properties and acoustic loss accompany the redistribution of domains (and strains) in the crystal during the first poling, and much smaller changes occur in subsequent electrical cycles. Polarized light microscopy confirms the occurrence of inhomogeneous strain due to motion of ferroelastic domains walls during the first poling. 180° polarization switching, which does not contribute to the elastic changes, becomes predominant after a few cycles, and pinning due to defects and localized strains cause enhancement of the ferroelectric coercivity.

RUS while *in situ* cycling electric field may open up new possibilities in, for example: (i) studies of engineered ferroelectric samples<sup>12</sup> where domain structures are prepared to favor a defined polarization switching process; (ii) exploration of the dependence of applied field orientation on the switching mechanism,<sup>22</sup> or on the elastic behavior near phase transitions,<sup>42,43</sup> (iii) identification of the elastic signatures of different possible switching pathways for lower symmetry phases;<sup>44,45</sup> and (iv) investigations of electric-field response of polar regions near ferroelastic domain walls in nonpolar materials.<sup>46–49</sup>

See [supplementary material](#) for the RUS measurements on sample A after annealing and description of supplementary videos taken on sample B.

## ACKNOWLEDGMENTS

This work was funded by EPSRC Grant Nos. EP/P024904/1 and ERC Starting Grant No. 680032, which are gratefully acknowledged. RUS facilities in Cambridge were established through grants from the Natural Environment Research Council (Grant Nos. NE/B505738/1 and NE/F017081/1) and the Engineering and Physical Sciences Research Council (Grant No. EP/I036079/1) to M.A.C. G.F.N. would like to thank the Royal Commission for the Exhibition of 1851 for the award of a Research Fellowship. J.E.T. and G.F.N. are grateful to Nadia Stelmashenko for useful discussions. X.M. is grateful for support from the Royal Society.

## REFERENCES

<sup>1</sup>Y. Ishibashi and Y. Takagi, *J. Phys. Soc. Jpn.* **31**, 506 (1971).

<sup>2</sup>J. F. Scott, *Ferroelectrics* **503**, 117 (2016).

<sup>3</sup>W. J. Merz, *Phys. Rev.* **88**, 421 (1952).

<sup>4</sup>S. Wada, K. Yako, H. Kakemoto, T. Tsurumi, and T. Kiguchi, *J. Appl. Phys.* **98**, 014109 (2005).

<sup>5</sup>X. Ren, *Nat. Mater.* **3**, 91 (2004).

<sup>6</sup>J. M. Hu, Z. Li, L. Q. Chen, and C. W. Nan, *Nat. Commun.* **2**, 553 (2011).

<sup>7</sup>W. Eerenstein, M. Wiora, J. L. Prieto, J. F. Scott, and N. D. Mathur, *Nat. Mater.* **6**, 348 (2007).

<sup>8</sup>R. O. Chherifi, V. Ivanovskaya, L. C. Phillips, A. Zobelli, I. C. Infante, E. Jacquet, V. Garcia, S. Fusil, P. R. Briddon, N. Guiblin, A. Mougin, A. A. Únal, F. Kronast, S. Valencia, B. Dkhil, A. Barthélémy, and M. Bibes, *Nat. Mater.* **13**, 345 (2014).

<sup>9</sup>M. Ghidini, F. Maccherozzi, X. Moya, L. C. Phillips, W. Yan, J. Soussi, N. Métallier, M. E. Vickers, N. J. Steinke, R. Mansell, C. H. W. Barnes, S. S. Dhesi, and N. D. Mathur, *Adv. Mater.* **27**, 1460 (2015).

<sup>10</sup>T. H. E. Lahtinen, K. J. A. Franke, and S. van Dijken, *Sci. Rep.* **2**, 258 (2012).

<sup>11</sup>J. F. Scott and C. A. Paz de Araujo, *Science* **246**, 1400 (1989).

<sup>12</sup>Y. W. Li, J. F. Scott, D. N. Fang, and F. X. Li, *Appl. Phys. Lett.* **103**, 232901 (2013).

<sup>13</sup>M. Hayashi, S. Imaizumi, and R. Abe, *Jpn. J. Appl. Phys.* **3**, 637 (2005).

<sup>14</sup>Y. A. Genenko, J. Glaum, M. J. Hoffmann, and K. Albe, *Mater. Sci. Eng., B* **192**, 52 (2015).

<sup>15</sup>W. J. Merz, *Phys. Rev.* **95**, 690 (1954).

<sup>16</sup>E. A. Little, *Phys. Rev.* **98**, 978 (1955).

<sup>17</sup>J. Fousek and B. Březina, *Czech. J. Phys.* **11**, 344 (1961).

<sup>18</sup>X. Y. Qi, H. H. Liu, and X. F. Duan, *Appl. Phys. Lett.* **89**, 092908 (2006).

<sup>19</sup>Z. H. Zhang, X. Y. Qi, and X. F. Duan, *Appl. Phys. Lett.* **89**, 242905 (2006).

<sup>20</sup>J. Shieh, J. H. Yeh, Y. C. Shu, and J. H. Yen, *Appl. Phys. Lett.* **91**, 062901 (2007).

<sup>21</sup>B. Jiang, Y. Bai, W. Chu, Y. Su, and L. Qiao, *Appl. Phys. Lett.* **93**, 152905 (2008).

<sup>22</sup>F. Li, Z. Xu, X. Wei, X. Yao, and L. Jin, *Appl. Phys. Lett.* **93**, 192904 (2008).

<sup>23</sup>E. K. H. Salje, D. Xue, X. Ding, K. A. Dahmen, and J. F. Scott, *Phys. Rev. Mater.* **3**, 014415 (2019).

<sup>24</sup>M. A. Carpenter, *J. Phys.: Condens. Matter* **27**, 263201 (2015).

<sup>25</sup>M. A. Carpenter, A. Buckley, P. A. Taylor, and T. W. Darling, *J. Phys.: Condens. Matter* **22**, 035405 (2010).

<sup>26</sup>J. F. Scott, E. K. H. Salje, and M. A. Carpenter, *Phys. Rev. Lett.* **109**, 187601 (2012).

<sup>27</sup>E. K. H. Salje, M. A. Carpenter, G. F. Nataf, G. Picht, K. Webber, J. Weerasinghe, S. Lisenkov, and L. Bellaiche, *Phys. Rev. B* **87**, 014106 (2013).

<sup>28</sup>M. A. Carpenter, J. F. J. Bryson, G. Catalan, S. J. Zhang, and N. J. Donnelly, *J. Phys.: Condens. Matter* **24**, 045902 (2012).

<sup>29</sup>G. F. Nataf, Q. Li, Y. Liu, R. L. Withers, S. L. Driver, and M. A. Carpenter, *J. Appl. Phys.* **113**, 124102 (2013).

<sup>30</sup>A. Migliori and J. D. Maynard, *Rev. Sci. Instrum.* **76**, 121301 (2005).

<sup>31</sup>E. K. H. Salje and W. T. Lee, *Nat. Mater.* **3**, 425 (2004).

<sup>32</sup>R. C. Miller and A. Savage, *Phys. Rev.* **115**, 1176 (1959).

<sup>33</sup>C. Mathieu, C. Lubin, G. Le Doueff, M. Cattelan, P. Gemeiner, B. Dkhil, E. K. H. Salje, and N. Barrett, *Sci. Rep.* **8**, 13660 (2018).

<sup>34</sup>Y. W. Li and F. X. Li, *Appl. Phys. Lett.* **104**, 042908 (2014).

<sup>35</sup>B. B. A. Fotčenkov, *Czech. J. Phys.* **14**, 21 (1964).

<sup>36</sup>M. Dawber, A. Gruverman, and J. F. Scott, *J. Phys.: Condens. Matter* **18**, L71 (2006).

<sup>37</sup>B. Meyer and D. Vanderbilt, *Phys. Rev. B* **65**, 104111 (2002).

<sup>38</sup>C. Brennan, *Ferroelectrics* **150**, 199 (1993).

<sup>39</sup>X. Y. Li, Q. Yang, J. X. Cao, L. Z. Sun, Q. X. Peng, Y. C. Zhou, and R. X. Zhang, *J. Phys. Chem. C* **122**, 3091 (2018).

<sup>40</sup>S. Tsurekawa, H. Hatao, H. Takahashi, and Y. Morizono, *Jpn. J. Appl. Phys.* **50**, 09NC02 (2011).

<sup>41</sup>F. Fang, W. Yang, F. C. Zhang, and H. S. Luo, *J. Am. Ceram. Soc.* **88**, 2491 (2005).

<sup>42</sup>X. Moya, E. Stern-Taulats, S. Crossley, D. González-Alonso, S. Kar-Narayan, A. Planes, L. Mañosa, and N. D. Mathur, *Adv. Mater.* **25**, 1360 (2013).

<sup>43</sup>N. Barrett, J. Dionot, D. Martinotti, E. K. H. Salje, and C. Mathieu, *Appl. Phys. Lett.* **113**, 022901 (2018).

<sup>44</sup>P. Zhao, M. Bao, A. Bur, J. L. Hockel, K. Wong, K. P. Mohanchandra, C. S. Lynch, and G. P. Carman, *J. Appl. Phys.* **109**, 124101 (2011).

<sup>45</sup>S. H. Baek and C. B. Eom, [Philos. Trans. R. Soc., A](#) **370**, 4872 (2012).

<sup>46</sup>L. Goncalves-Ferreira, S. A. T. Redfern, E. Artacho, and E. K. H. Salje, [Phys. Rev. Lett.](#) **101**, 097602 (2008).

<sup>47</sup>E. K. H. Salje, M. Alexe, S. Kustov, M. C. Weber, J. Schiemer, G. F. Nataf, and J. Kreisel, [Sci. Rep.](#) **6**, 27193 (2016).

<sup>48</sup>B. Casals, A. Schiaffino, A. Casiraghi, S. J. Hämäläinen, D. López González, S. van Dijken, M. Stengel, and G. Herranz, [Phys. Rev. Lett.](#) **120**, 217601 (2018).

<sup>49</sup>D. Pesquera, M. A. Carpenter, and E. K. H. Salje, [Phys. Rev. Lett.](#) **121**, 235701 (2018).